

Quantifying the uncertainty in passive microwave snow water equivalent observations

James L. Foster^{a,*}, Chaojiao Sun^{b,c}, Jeffrey P. Walker^d, Richard Kelly^{a,c}, Alfred Chang^a, Jiarui Dong^{a,c}, Hugh Powell^{a,e}

^aCode 974, Hydrological Sciences Branch, Laboratory for Hydrospheric Processes, NASA Goddard Space Flight Center, Greenbelt, MD, 20771, USA

^bGlobal Modeling and Assimilation Office, NASA Goddard Space Flight Center, Greenbelt, MD, 20771, USA

^cGoddard Earth Sciences and Technology Center, University of Maryland Baltimore County, Baltimore, MD 21250, USA

^dDepartment of Civil and Environmental Engineering, University of Melbourne, Parkville, Victoria, 3010 Australia

^eScience Applications International Corporation, 4600 Powder Mill Road, Beltsville, MD 20705, USA

Received 2 February 2004; received in revised form 9 September 2004; accepted 11 September 2004

Abstract

Passive microwave sensors (PM) onboard satellites have the capability to provide global snow observations which are not affected by cloudiness and night condition (except when precipitating events are occurring). Furthermore, they provide information on snow mass, i.e., snow water equivalent (SWE), which is critically important for hydrological modeling and water resource management. However, the errors associated with the passive microwave measurements of SWE are well known but have not been adequately quantified thus far. Understanding these errors is important for correct interpretation of remotely sensed SWE and successful assimilation of such observations into numerical models.

This study uses a novel approach to quantify these errors by taking into account various factors that impact passive microwave responses from snow in various climatic/geographic regions. Among these factors are vegetation cover (particularly forest cover), snow morphology (crystal size), and errors related to brightness temperature calibration. A time-evolving retrieval algorithm that considers the evolution of snow crystals is formulated. An error model is developed based on the standard error estimation theory. This new algorithm and error estimation method is applied to the passive microwave data from Special Sensor Microwave/Imager (SSM/I) during the 1990–1991 snow season to produce annotated error maps for North America. The algorithm has been validated for seven snow seasons (from 1988 to 1995) in taiga, tundra, alpine, prairie, and maritime regions of Canada using in situ SWE data from the Meteorological Service of Canada (MSC) and satellite passive microwave observations. An ongoing study is applying this methodology to passive microwave measurements from Scanning Multichannel Microwave Radiometer (SMMR); future study will further refine and extend the analysis globally, and produce an improved SWE dataset of more than 25 years in length by combining SSMR and SSM/I measurements.

Published by Elsevier Inc.

Keywords: Snow cover; Snow water equivalent; Passive microwave; Uncertainty; Observation errors; SMMR; SSM/I

1. Introduction

Snow plays an important role in the global energy and water budgets, as a result of its high albedo and thermal and water storage properties. Snow is also the largest varying

landscape feature of the Earth's surface. For example, in North America, the snow cover extent may vary from greater than 50% to less than 5% in the course of six months (Hall et al., 2002), and the snow water equivalent (hereafter referred to as SWE) of mid-latitude snowpacks can be reduced by as much as 100 mm in less than 6 days. Furthermore, snow depth and SWE, as well as snow cover extent, are important contributors to both local and remote climate (Gong et al., 2004). Thus, knowledge of snow

* Corresponding author. Tel.: +1 301 614 5769; fax: +1 301 614 5808.

E-mail address: James.L.Foster@nasa.gov (J.L. Foster).

extent and SWE are important for climate change studies and applications such as flood forecasting.

Despite its importance, the successful forecasting of snowmelt using atmospheric and hydrologic models is challenging. This is due to the imperfect knowledge of snow physics and simplifications used in the model, as well as errors in the model forcing data. Furthermore, the natural spatial and temporal variability of snow cover is characterized at space and time scales below those typically represented by models. Snow model initialization based on model spin-up will be affected by these errors. By assimilating snow observation products into land surface models, the effects of model initialization error may be reduced (Sun et al., 2004).

A critical requirement for successful assimilation of snow observations into models is an accurate knowledge of the observation errors. While it is possible to directly replace modeled states with observed states, this does not take into account the fact that model predictions and remotely sensed observations contain different amounts of error. In state-of-art data assimilation, error statistics of the observational data are required so that the correct weighting between observations and model estimates may be applied. Furthermore, in order for the remotely sensed SWE observations to be useful for climate modelers, water resource managers, and flood forecasters, it is necessary to have a quantitative, rather than qualitative, estimate of the uncertainty. A framework is needed to estimate SWE and its associated errors over large geographic areas.

In situ SWE data are poorly distributed globally and collected irregularly (Robinson et al., 1993). Passive microwave remote sensors onboard satellites provide an all-weather global SWE observation capability day or night. Brightness temperatures from different channels of satellite passive microwave sensors (hereafter referred to as PM) can be used to estimate SWE (or snow depth with knowledge of the snow density), and hence snow cover extent. This is a significant advantage over infrared sensors, which only work under cloud-free conditions, and visible sensors, which also require daylight to observe terrestrial features. More importantly, PM sensors provide estimates of the snow mass and not just snow cover extent. However, there are errors associated with the PM measurements. In order for the remotely sensed SWE observations to be useful for climate modelers, water resource managers, and flood forecasters, it is necessary to have both an unbiased SWE estimate and a quantitative, rather than qualitative, estimate of the uncertainty. This is a critical requirement for successful assimilation of snow observations into land surface models.

For most PM algorithms, the effects of vegetation cover and snow grain size variability are the main source of error in estimating SWE. Of lesser concern are the effects of topography and atmospheric conditions. A major assumption made in a number of PM algorithms is that vegetation cover does not affect the SWE estimates. In fact, it can have a significant impact on the accuracy of SWE estimates. In

densely forested areas, such as the boreal forest of Canada, the underestimation of SWE from retrieval algorithms can be as high as 50% (Chang et al., 1996). Other factors such as topography and ice crusts effect PM retrievals but to a lesser extent than forests and crystal size.

The purpose of this paper is to explore a methodology for deriving unbiased PM SWE observations and associated uncertainty estimates. Errors due to simplifying assumptions of the retrieval algorithm are quantified. The 1990–1991 snow season is examined in detail as an example. PM SWE data from Special Sensor Microwave/Imager (SSM/I) for this snow season and their associated uncertainty are analyzed throughout North America. SSM/I data from seven snow seasons (from 1988 to 1995) are examined to evaluate our approach and validate our algorithm. We have focused on North America due to the availability of extensive in situ SWE data and abundance of field campaigns relative to the rest of the world. A future study will extend our analysis globally.

2. PM radiometry

Microwave emission from a snow layer over a ground medium consists of contributions from the snow itself and from the underlying ground. Both contributions are governed by the transmission and reflection properties of the air–snow and snow–ground boundaries, and by the absorption/emission and scattering properties of the snow layers (Chang et al., 1976; Wiesman & Mätzler, 1999). Snow crystals essentially scatter part of the cold sky radiation, which reduces the upwelling radiation measured with a radiometer (Schmugge, 1980). The deeper or more compact the snowpack is, the more snow crystals are available to scatter the upwelling microwave energy. It is this interaction property that is used to estimate snow mass.

If a snowpack is not too shallow (for example, the thickness of the snowpack is greater than 5 cm or equivalently, the snowpack contains more than about 10 mm SWE), scattering of naturally emitted microwave radiation by snow crystals occurs and can be detected at frequencies greater than about 25 GHz. Otherwise, the snow will be virtually transparent. By comparing brightness temperatures detected at an antenna at frequencies greater than 25 GHz (typically scattering dominated) with those brightness temperatures detected at frequencies less than 25 GHz (typically emission dominated), it is possible to identify scattering surfaces. Generally, the strength of scattering signal is proportional to the SWE, and it is this relationship that forms the basis for estimating the water equivalent (or thickness) of a snow pack (Chang et al., 1976; Kelly and Chang, 2003; Pulliainen & Hallikainen, 2001; Tsang et al., 2000; Ulaby & Stiles, 1980).

From November 1978 to the present, the Scanning Multichannel Microwave Radiometer (SMMR) instrument on the Nimbus-7 satellite, and the SSM/I on the Defense

Meteorological Satellite Program (DMSP) series of satellites have acquired PM data every other day that can be used to estimate SWE. The SMMR instrument failed in 1987, the year the first SSM/I sensor was placed in orbit. On SMMR, the channels most useful for snow observations are the 18 and 37 GHz channels. For the SSM/I, the frequencies are slightly different (19.35 and 37.0 GHz). Additionally, an 85 GHz channel is available on the SSM/I. This frequency has been demonstrated to be beneficial in detecting shallow snowpacks (less than 5 cm thick) if the atmosphere is relatively free of clouds (Foster et al., 1996). PM data from SSM/I for most places on the globe are available each day. The swath data (obtained from Remote Sensing Systems) are projected into $0.5^\circ \times 0.5^\circ$ longitude Equal Area Scalable Earth Grid (EASE-grid). These grid cells uniformly subdivide a polar stereographic map according to the geographic coordinates of the center of the field of view of the radiometers. Overlapping data in cells from separate orbits are averaged to give a single brightness temperature, assumed to be located at the center of the cell (Armstrong & Brodzik, 1995; Chang & Rango, 2000). With the launch of Earth Observing System (EOS) Aqua satellite in May 2002, high-quality PM SWE observations are available from its Advanced Microwave Scanning Radiometer for EOS (AMSR-E) instrument. An overview of the characteristics of the SMMR, SSM/I, and AMSR instruments is given in Table 1.

There is some question about the effect of polarization on snow depth and SWE estimation using PM data. From ground based microwave measurements, Matzler (1987) showed that horizontally polarized brightness temperatures at 19 and 37 GHz are slightly more sensitive to snowpack stratigraphy than the vertically polarized brightness temperatures. For spaceborne passive microwave observations over large footprints, however, Rango et al. (1979) demonstrated that brightness temperatures at horizontal and vertical polarization have very similar relationships with snow depth or snow water equivalent. Furthermore, when using a Tb

difference algorithm at these two frequencies, the snowpack stratigraphy effects in one-channel frequency will be very similar to the effects in the other (Kelly et al., 2003).

Melt water in the snowpack can raise the microwave brightness temperature, especially at frequencies above about 30 GHz, since water droplets emit rather than scatter microwave radiation. While SWE information can be difficult to extract under these conditions, it is possible to use this characteristic to extract information on snowmelt status (Walker & Goodison, 1993). In order to minimize the effect of these conditions on SWE estimates, only nighttime data have been used in this paper. This helps to ensure, but cannot guarantee, that whatever snow has melted during the day will be refrozen at night (Derksen et al., 2000).

3. A new retrieval algorithm

3.1. A commonly used SWE algorithm

A commonly used SWE retrieval algorithm was developed by Chang et al. (1987), where brightness temperature differences between the 19 (or 18 GHz for SMMR) and 37 GHz channels are multiplied by a constant c_0 determined from radiative transfer model experiments of snow. The simple algorithm for SWE retrieval is

$$W = c_0(T_{19} - T_{37}) \text{ [mm]}, \quad (1)$$

where W is snow water equivalent in mm, c_0 is 4.8 mm K^{-1} for SSM/I (4.77 for SMMR), and T_{19} and T_{37} are the horizontally polarized brightness temperatures at 19 (or 18 GHz for SMMR) and 37 GHz, respectively. Using 19 vs. 18 GHz has a very small effect on the algorithm, since the penetration for both frequencies is nearly identical at an incidence angle of 50° . In deriving the retrieval algorithm (1), the snow grain radius and snow density was assumed to be 0.3 mm and 300 kg m^{-3} , respectively.

The performance of this algorithm is similar when either vertical or horizontal polarizations are utilized—horizontal polarization was used in this study (Rango et al., 1979). If the brightness temperature from the 19 GHz (or 18 GHz) channel is less than that from the 37 GHz channel, then the snow depth and SWE are set to 0. To derive snow depth, SWE is simply divided by the snow density. It has been determined that, in general, a snow density value of 300 kg m^{-3} is representative of mature mid winter snow packs in North America (Foster et al., 1996). Therefore, the equivalent snow depth retrieval algorithm can be obtained by modifying the coefficient c in (1) such that its value is 1.60 cm K^{-1} .

In the wavelength range between about 0.8 ($\sim 37 \text{ GHz}$) and 2.0 cm ($\sim 15 \text{ GHz}$) and for snow crystal sizes normally encountered in snowpacks (diameter of about 0.1 to 0.5 mm), nearly all of the microwave radiation emanates from a layer less than 10 m in thickness (Chang et al., 1976). Because of low loss when snow is dry, part of the radiation emitted by the underlying ground is scattered within the

Table 1
Characteristics of passive microwave sensors SMMR, SSM/I, and AMSR-E

	SMMR	SSM/I	AMSR-E
Platform	Nimbus-7	DMSP F-8, 11, 13	Aqua
Period of operation	1979–1987	1987–present	2002–present
Data acquisition	every other day	daily	daily
Swath width (km)	780	1400	1600
Frequency (GHz)	18.0 37.0	19.35 37.0	18.7 36.5
Spatial resolution (km)	60×40 (18 GHz) 30×20 (37 GHz)	69×43 (19.4 GHz) 37×29 (37 GHz)	28×16 (19.7 GHz) 14×8 (36.5 GHz)
Polarization	H&V	H&V	H&V
Orbital timing (Eq. crossing; for minimum temperature)	Midnight	6:00 a.m.	1:30 a.m.
Incidence angle	51°	53°	53°

snowpack and part contributes to the observed signal when the total snow depth is less than 10–100 times the microwave wavelength (Rango, 1983). Therefore, in most cases, additional scattering does not result when snow thickness exceeds 0.8 m—the approximate “saturation” limit for 37 GHz frequencies. For most locations in North America, usually, snow does not accumulate to these depths over an entire PM pixel (37 km×28 km for SSM/I). In portions of the Rocky Mountains and the Alaska Ranges, and perhaps in a few isolated areas in the boreal forests of Quebec, depths of 1 m or more can be reached, but our analysis indicates that these pixels make up less than 2% of all the pixels in North America.

3.2. A new retrieval algorithm

To account for the impact of vegetation cover and the evolution of the snow crystals with the progression of snow season, we modify the simple retrieval algorithm (1), by using forest cover information from the International Geosphere–Biosphere Program (IGBP) Land Cover Data Set (Loveland et al., 2000), and snow crystal information based on the work by Sturm et al. (1995; see Fig. 1). The details are described below.

3.2.1. Impact of vegetation cover

The primary source of error in PM SWE retrieval is the masking effect of vegetation. Microwave emission from overlying forest canopy can overwhelm the scattering signal from the snowpack, thus reduce the brightness temperature difference term in (1) (Chang et al., 1996). In the PM portion of the electromagnetic spectrum, the underestimation error in the boreal forest can be as high as 50% (Brown et al.,

2003). In the tundra and prairie areas, the SWE estimates are more reliable because vegetation is sparse, thus there is little extraneous emission. In fact, dense vegetation not only creates problems for snow retrievals in the microwave part of the spectrum but also in the visible wavelengths as well. Hall et al. (2001, 2002) found that when employing the MODerate Resolution Imaging Spectroradiometer (MODIS) snow algorithm, snow-detection errors were as high as 43% in densely forested areas of the boreal forest in Canada.

The importance of land cover on SWE algorithms has been well recognized. The Meteorological Service of Canada (MSC) has developed a suite of land cover-sensitive empirical SWE algorithms for passive microwave retrievals (Goita et al., 2003). The land cover is divided into four categories: Open, Coniferous forest, Deciduous forest, and Sparse forest. A different empirical algorithm is applied to each category. Derksen et al. (2003) evaluated the MSC algorithms for 18 winter seasons in the western Canada using data from SMMR and SSM/I. The algorithms perform well in open and sparsely forested regions as compared to the in situ SWE data, but have significant difficulty in densely forested or deep snow-covered areas.

To address continental-scale SWE estimations, we use a single parameter (percentage of forest cover) to parameterize the effect of vegetation cover. For each forested pixel, a *fractional forest cover* is calculated using the IGBP Land Cover Data Set (Loveland et al., 2000). These data, at 1 km×1 km, are averaged to the 0.5°×0.5° latitude/longitude grid used in this study. The percentage of forest cover in a PM pixel was calculated from the total number of forest classification pixels at 1 km divided by the total number of pixels. Underestimation of SWE due to forest cover is then parameterized empirically.

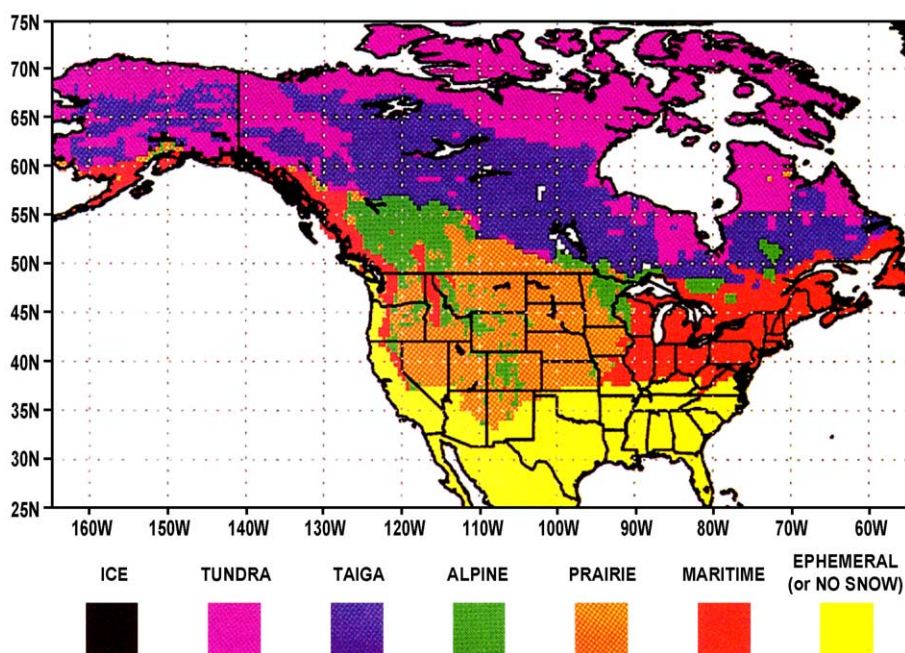


Fig. 1. Snow class distribution based on climate variables in North America (from Sturm et al., 1995).

This is a simplified approach since it assumes fractional forest cover in a pixel is the most relevant factor that affects the microwave emission by vegetation cover. In fact, forest inventory variables (canopy volume and stem closure) that characterize forest structure are more relevant for passive microwave emission from ground, not simply the fraction of forest cover. Crown closure, basal area (the cross sectional area of tree stems per unit ground area), and foliage biomass are directly related to microwave emission since they are all inversely related to visible reflectance (Franklin, 1986). At the northern edge of the boreal forest, a pixel that is covered by sparsely spaced stunted conifers might be considered completely forested and can have very different microwave emissions as compared to a highly forested taiga pixel covered by large trees in close proximity of one another. Additionally, a conifer is likely to be more emissive than a deciduous tree in mid-winter. Due to lack of in situ data on detailed forest characteristics in the North America, the influence of latitude or species was not considered in this study.

For every 10th percentile of the fractional forest cover, an ad hoc underestimation error of SWE by PM retrieval from (1) is assigned (Fig. 2a). Since the largest underestimation error occurs when a pixel is highly forested, i.e., its fractional forest cover is between 80% and 100%, the underestimation by (1) in this case is set to 50% of “true” SWE. On the other hand, in tundra regions, where by definition forests are not present (but shrubs and grasses thrive in this region), the underestimation error is set to 5%.

As we recognize that the underestimation error can vary depending on the type of vegetation and stem volume for a given fractional forest cover, which are not considered in the current approach, we also assign an error bar to the underestimation error (Fig. 2a). Small error bars are assigned to small values (below 20%) and high values (above 80%) of fractional forest cover, while large error bars are assigned to pixels with medium values of fractional forest cover. This is because uncertainty is relatively small when a pixel is barely forested, and for a densely forested pixel, the underestimation could be reasonably quantified. When a pixel is more mixed with bare ground and forest, it is harder to untangle the contribution of the PM signal due to scattering from the underlying snow and emission from trees.

These values are currently our best guess, since no studies exist to provide such bounds. Nevertheless, these underestimation errors and error bars were partly assigned based on previous field work in the BOREAS project (see Chang et al., 1996) and analysis of visible and microwave satellite observations in the boreal forests (Foster et al., 1991; Hall et al., 1982; Robinson & Kukla, 1985; Scialdone & Robuck, 1987). When more accurate limits become available, they can be replaced and more rigorous uncertainty estimates can be achieved. Recent field experiments, such as the Cold Land Processes Field Experiment (CLPX), holds great promise in rigorously validating passive microwave SWE retrievals and their error ranges with carefully surveyed in situ SWE.

Using the assigned estimation error, a modified SWE algorithm that is sensitive to vegetation cover can be derived. Denote the estimated SWE for a pixel by (1) as W , the SWE value that has been corrected for forest influence as W_F , and the under- or over-estimation error as ϵ , then

$$W_F - W = \epsilon W_F \tag{2}$$

That is,

$$W_F = W / (1 - \epsilon) \tag{3}$$

Denote F as

$$F = 1 / (1 - \epsilon), \tag{4}$$

then an algorithm that accounts for vegetation cover is

$$W_F = F c_0 (T_{19} - T_{37}) \text{ [mm]} \tag{5}$$

We refer to F as the “forest factor” hereafter. Fig. 2b shows F as a function of fractional forest cover in North America.

3.2.2. Impact due to growth of snow crystals

The second major source of SWE error results from the assumption that snow crystal size remains constant throughout the snow season and is uniform globally. This assumption is reflected in the original SWE retrieval algorithm (1) where c_0 is a constant. In reality, snow crystal sizes vary considerably over time and space. The microwave response of snow has been found to be very sensitive to crystal size, although not sensitive to crystal shapes (Foster

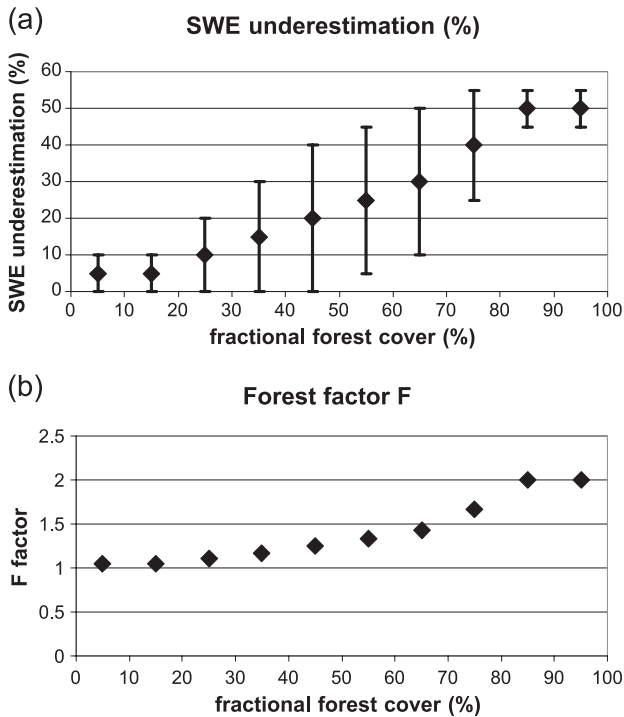


Fig. 2. (a) Underestimation of SWE due to forest cover. The error bars denote uncertainty of the underestimation. (b) The forest factor F as a function of fractional forest cover.

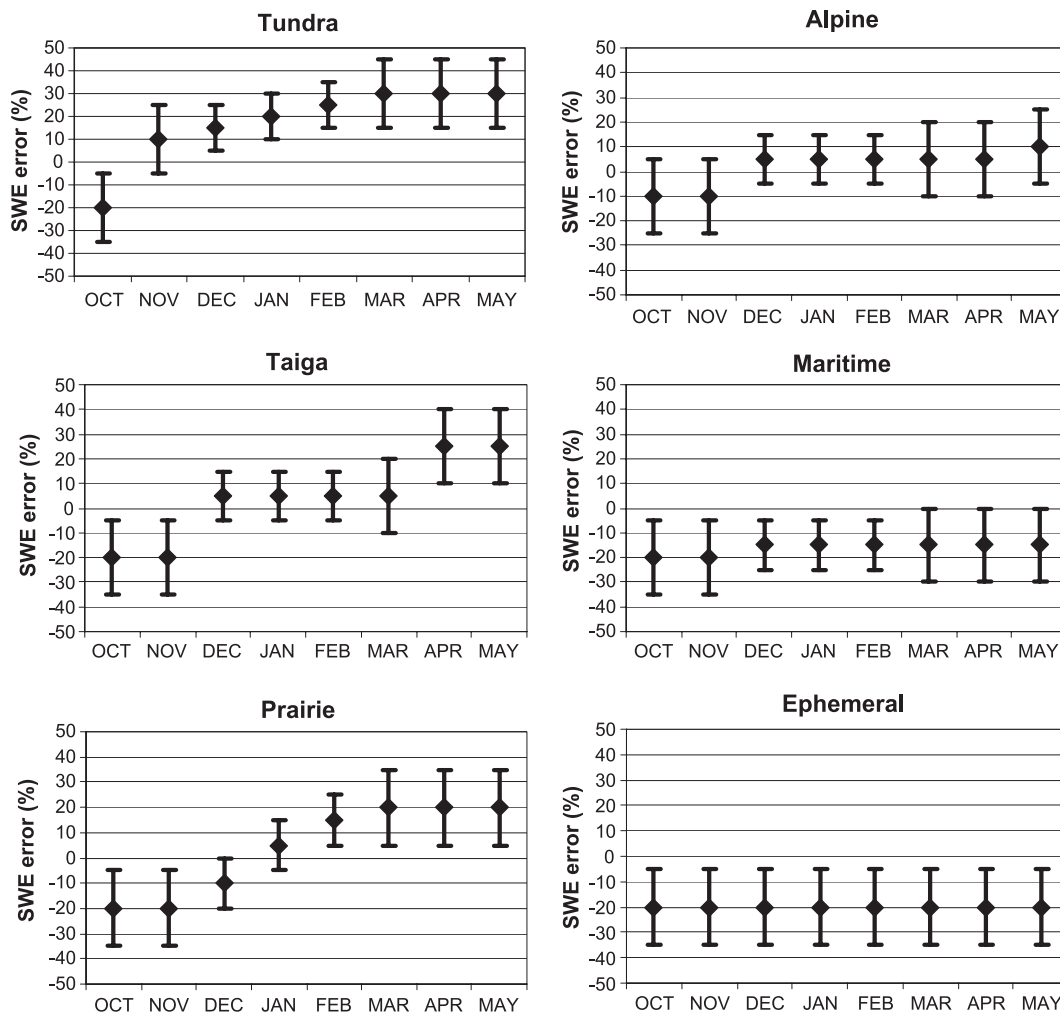


Fig. 3. SWE overestimation or underestimation error (shown in diamonds) for the six Sturm classes due to the assumption of constant grain size. Error bars denote uncertainty in these error estimates.

et al., 1999). In most snowpacks, constructive metamorphism is greater than destructive metamorphism, so the net result is that, on average, crystals either grow or stay at about the same size during the snow season (Colbeck, 1982). Consequently, algorithm (1) generally overestimates SWE (if vegetation effect is accounted for) because microwave scattering increases as the crystals grow larger.

Here we evolve the coefficient c in (5) temporally and spatially, based on snow crystal characteristics in different geographical and climate regions and our understanding of how they evolve with time. The characterization of seasonal snowpacks in the North America is from Sturm et al. (1995) who analyzed relations between textural and stratigraphic characteristics of snow layers and climate variables, and categorized snow packs in the North America and Eurasia into six classes (excluding continental ice caps and ocean/water bodies): tundra, taiga (Russian word for moist, subarctic coniferous forest), alpine, prairie, maritime, and ephemeral (Fig. 1). For simplicity, we will refer to these classes as *Sturm* classes hereafter.

To derive a spatially and temporally varying coefficient c , we start by estimating how much error there is when using (5), which still assumes constant crystal size of 0.3 mm in radius. Keep in mind, we now assume the influence of vegetation cover has been taken care of. A monthly error value γ is assigned to each Sturm class (Fig. 3). If the error is 20%, it means we expect (5) to overestimate the “true” SWE by 20%. Note negative error values of γ denote underestimation of SWE by (5). The “true” SWE value W^t is then

$$W^t = W_F - \gamma W_F = (1 - \gamma) W_F, \quad (6)$$

where W_F is the SWE value from (5). The “true” SWE value is

$$W^t = (1 - \gamma) F c_0 (T_{19} - T_{37}) \quad (7)$$

Denote a varying coefficient c as,

$$c = (1 - \gamma) c_0 \quad (8)$$

The new algorithm is now

$$W = Fc(T_{19} - T_{37}) \tag{9}$$

where we have dropped the superscript “*t*”; *F* and *c* are time- and space-varying coefficients, with *F* from (4) and *c* from (8).

In areas that favor crystal growth, e.g., with large air temperature gradients, (northern interior climates—taiga, tundra, and prairie snow classes), the rate of growth and the associated crystal size errors are typically larger. As the snow season progresses, the overestimation by (5) in these classes increases because (5) assumes that snow crystals do not grow with time. The greatest overestimation occurs in the tundra snow and the least in maritime or ephemeral snow. The exception occurs for the months of October and November, when SWE is mostly underestimated by (5). That is, because the snow cover is usually shallow (<5 cm) at the beginning of the snow season, microwave radiation at all observed frequencies can pass through the snowpack virtually unimpeded, therefore snow is underestimated.

These error values are assigned in an ad hoc way which represents our best guess. As with the case of deriving *F*, these values are assigned based on various field campaign results with snow crystal samples collected and analyzed, as well as subjective analysis based on previous work and field experiences in Colorado, Wisconsin, North Dakota, Alaska, and Saskatchewan (see for example, Chang et al., 1982, 1985, 1986, 1996; Hall et al., 1986, 1991). These error estimates can be refined once new field campaign results become available.

To quantify the uncertainty in the new algorithm (9), error bars are assigned to these error estimates (Fig. 3). For example, the overestimation error for the prairie snow class in March is set to 20%, yet the actual underestimation could vary between 5% and 35%. A 15% error bar is thus assigned to the prairie class in March. The uncertainty of the overestimation is slightly higher in those classes where crystal growth is a dominant snowpack characteristic (tundra, taiga, and prairie classes) and at those times of year where crystals grow most rapidly.

Fig. 4 shows different values of *c* for each *Sturm* class for each month of the snow season (October to May) for North America, as calculated from (8). The coefficient *c* often decreases from autumn through spring because crystal size in mature snowpacks usually increases during this period. The original constant coefficient *c*₀ (4.8 mm) is associated with an average crystal size of 0.3 mm (radius). For *c* values smaller than 4.8, the algorithm assumes larger crystals.

It should be noted that there can be a tremendous size range of snow crystals from the bottom to the top of a snowpack. Depth hoar crystals may have a radius of 5 mm, whereas fresh powder snow consists of very fine crystals (1 mm in radius). While these are extreme cases, the variety of crystal sizes in a mature mid-winter snowpack in the interior of North America can nonetheless be enormous. Reconciling an “average” crystal size is difficult indeed. It may be that the median or the most frequently observed size (mode) is a better statistic. Yet, even though a single value for crystal size may not be entirely representative of the myriad crystals encountered within a snowpack, nevertheless, we circumvent this

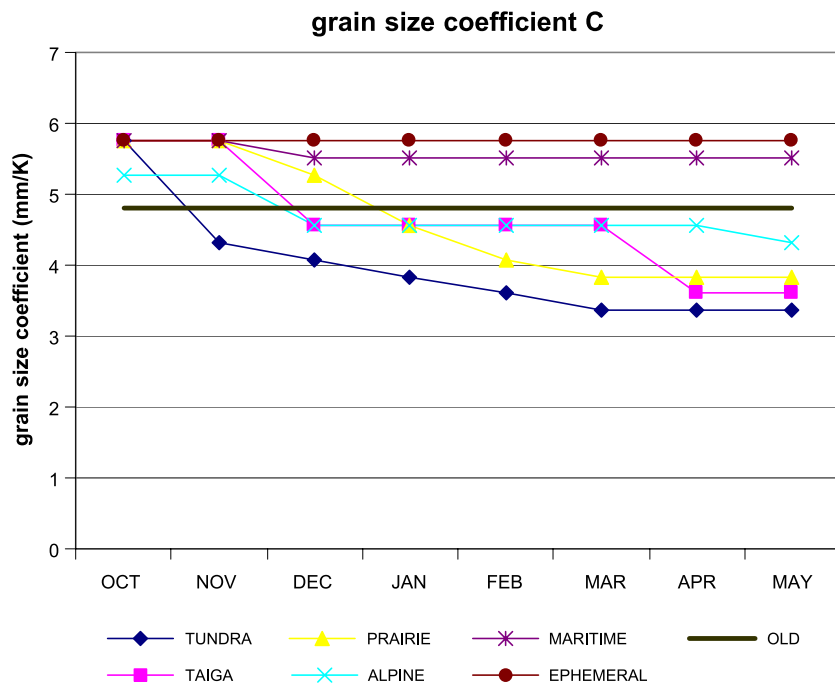


Fig. 4. Grain size coefficient *c* (in mm K⁻¹) as a function of time for six *Sturm* classes. The constant value (4.8 mm K⁻¹) used in the original algorithm is also plotted and labeled as “OLD”.

problem by using an empirical and ad hoc approach in deriving c . To rigorously derive c , extensive calibration and validation are required between PM estimates and ground measurements (the “ground truth”).

In summary, to compute PM SWE value for each pixel using (9), the forest factor F is determined based on the forest cover fraction of this pixel, and the coefficient c value is assigned based on its snow class category and time of the year. The purpose of introducing the forest factor F and time- and space-varying c in (9) is to correct the systematic errors in (1). Note that we have assumed that the forest masking and snow crystal size effect independently affects the algorithm, and their total effects can be combined in a multiplicative way to correct the error.

4. Error analysis

We use standard error propagation theory (e.g., [Heuvelink, 1998](#)) to quantify the uncertainty associated with the new SWE retrieval algorithm (9), and assume that errors from different sources are uncorrelated, which is defensible. The uncertainty consists of error propagation terms and model error terms for unaccounted processes. The error propagation terms include brightness temperature calibration errors for the 19 and 37 GHz bands, errors due to forest cover and snow crystal effects. The model error terms include errors due to topography (roughness and incidence angle), atmospheric, and calibration errors in the radiative transfer model on which (1) is based. The uncertainty in SWE is calculated as

$$\sigma_w^2 = \underbrace{\left(\frac{\partial W}{\partial c}\right)^2 \sigma_c^2 + \left(\frac{\partial W}{\partial F}\right)^2 \sigma_F^2 + \left(\frac{\partial W}{\partial T_{19}}\right)^2 \sigma_{T_{19}}^2 + \left(\frac{\partial W}{\partial T_{37}}\right)^2 \sigma_{T_{37}}^2}_{\text{Error Propagation Term}} + \underbrace{\sigma_{\text{topography}}^2 + \sigma_{\text{atmosphere}}^2 + \sigma_{\text{calibration}}^2}_{\text{Model Error Term}} \quad (10)$$

where σ denotes the standard deviation of each of the component factors (c , F , T_{19} , T_{37} , and W). When retrieving snow depth from PM measurements, the uncertainty in snow density also needs to be included as an error propagation term. This is not considered here since we focus on SWE retrieval in this study.

Apply (9) into (10), we get

$$\sigma_W^2 = \underbrace{F^2(T_{19} - T_{37})^2 \sigma_c^2 + c^2(T_{19} - T_{37})^2 \sigma_F^2 + F^2 c^2 \sigma_{T_{19}}^2 + F^2 c^2 \sigma_{T_{37}}^2}_{\text{Error Propagation Term}} + \underbrace{\sigma_{\text{topography}}^2 + \sigma_{\text{atmosphere}}^2 + \sigma_{\text{calibration}}^2}_{\text{Model Error Term}} \quad (11)$$

Evaluation of the error propagation terms in (11) is relatively straightforward, requiring only differentiation of the algorithm in (9) and uncertainty estimates for the

algorithm inputs. However, evaluation of the model error terms is somewhat more difficult, with knowledge of the effect of each of the nonmodeled terms on SWE estimation required. A calibration uncertainty for the 19 and 37 GHz brightness temperature data of 1 K was used, and a calibration error of 5 mm by the radiative transfer model was applied (Chang, personal communication).

While atmospheric error is also included as a model error term, this effect is deemed negligible and omitted from the uncertainty analysis. This is because during the period when snow covers the ground, when clouds are present, they are almost always composed of minute ice crystals rather than water droplets. Since ice crystals have a similar response to the microwave signals at the two frequencies used to derive SWE, the error due to atmospheric emission is minimized.

Another source of uncertainty is the effect of relief or topography. Mountain ranges with significant relief (>500 m between adjacent pixels) can alter the microwave signal received at the antenna ([Matzler & Standley, 2000](#)). For example, mountain ranges perpendicular to the track of the satellite may have slightly lower (<5 K) brightness temperatures on the side of the range facing in the direction of the sensor than on the side facing away from the sensor. Inevitably, mixed pixel effects including forest cover variations in mountainous terrain and differences in snow crystal size with elevation will be more important than relief factors. Nevertheless, if no forests are present, and if changes in crystal size are negligible, then errors attributable to relief alone may need to be considered. This is beyond the scope of this paper and not considered here.

It is worth mentioning that wind and ice crusts can adversely affect PM retrievals. However, use of a single polarization in PM algorithms minimizes this concern, since this effect is only significant when brightness temperatures from different polarizations (vertical and horizontal) are used. Nonetheless, surface crusts occurring over large areas (multiple PM pixels) for extended periods (weeks), can confound PM algorithms, although it should be noted that this phenomenon does not occur routinely. Again, our focus in this study is on errors associated with forest cover and crystal size, which are major contributors to the PM SWE retrieval error.

5. Results

As a case study, we focus on snow season 1990–1991 in this section. We will examine other snow seasons in the Validation section later. We first present monthly SSM/I SWE maps in North America computed from the new algorithm (9). Then we compare the results between the old and new algorithms and discuss their differences. Finally, we evaluate the uncertainty associated with the new algorithm (9) using (11).

5.1. Monthly SWE during 1990–1991

Fig. 5 is a series of monthly maps from October 1990 through May 1991 showing the monthly average SWE in North America using (9). Note that pixels that mix with large water bodies have been designated as snow free, because PM measurements are contaminated by the emission of water in the pixels, although they may be snow-covered during much of the snow season. In October 1990, snow was mostly confined to the tundra region, and the maximum SWE was less than 90 mm. By November, the contiguous snow covered area had expanded southward toward the U.S./Canada border. Although SWE values were generally less than 120 mm, in a few locations in the taiga region (e.g., Yukon Territory and Alaska), they were over 180 mm.

By December, the area of contiguous snow stretched from the intermountain basins of the western U.S. across the central plains and into northern New England. However, the northern U.S. plains and southern Canadian prairies were still snow free. It is not unusual to find snow-free areas in the lee of the Rocky Mountains, because in this semiarid region, evaporation nearly always exceeds condensation, and sublimation (accelerated by persistent winds) can

quickly remove shallow snow cover. While the snowpack was still thin in the U.S., the snowpacks had grown thicker in the taiga and Canadian prairies, where some SWE values were greater than 150 mm.

By January 1991, the snowline had reached its maximum extent—it was positioned as far south as the southern plains of the U.S. The SWE had noticeably increased (compared to December SWEs) throughout North America. A large proportion of the Canadian taiga region now showed SWE values in excess of 200 mm. The SWE map for February is similar to that of January, but the areal extent of the snow cover is slightly less. Note that the snow-free area of the Great Plains had reappeared. By March, the snow line had started to retreat northward, and the snowpack had diminished in the U.S. Rockies and upper Mid West. However, in Canada, there was very little difference in SWE between February and March.

In April, the snow-covered area had further contracted—the contiguous snowline was now positioned near the U.S./Canada border. SWE values remained small (less than 30 mm) across the prairie regions, but were in excess of 90 mm almost everywhere in the boreal forest—some snowpacks still have SWE values greater than 150 mm. By May, the snowline had further migrated northward into the taiga

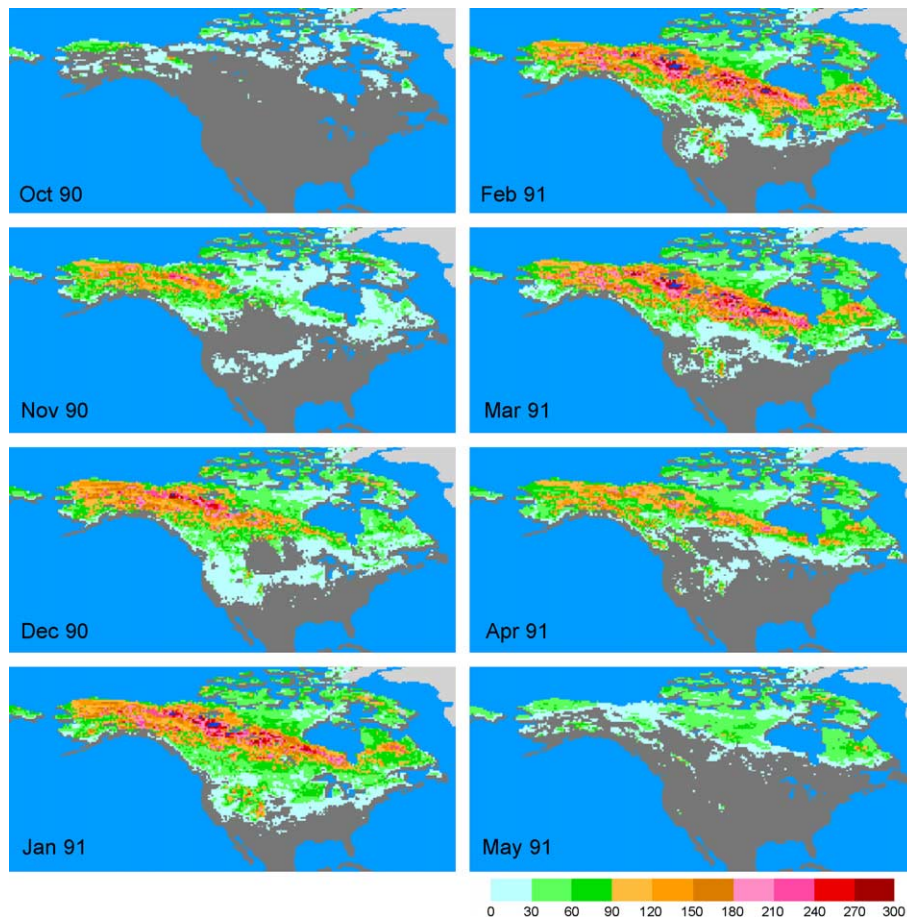


Fig. 5. SSM/I monthly SWE maps from October 1990 through May 1991. Gray-colored area is Greenland, and brown-colored area is snow-free.

region. At this time, SWE values were less than 60 mm in most taiga and tundra locations.

Weekly NOAA snow maps from October 1990 through May 1991, in general, compared favorably to the snow cover extent in Fig. 5 (not shown here). Although we compared monthly SWE maps with the weekly NOAA snow cover extent maps, nevertheless, the maps were in very close accord throughout the snow season (NOAA/NESDIS, 1990 and 1991).

5.2. Comparison of the new and old algorithms

Fig. 6 shows differences in SWE estimates by the new algorithm (9) and old algorithm (1). Positive (negative) values indicate new algorithm estimates more (less) snow than the old algorithm. If we treat the new algorithm as the “correct” algorithm, then positive values indicate underestimation by the old algorithm, and negative values indicate overestimation by the old algorithm. We should point out that we use the term “overestimation” and “underestimation” here as if the new algorithm gives the “true” value of SWE. However, this is only accurate when the new algorithm is rigorously validated with sufficient “ground truth” data.

Snow was underestimated using (1) in forested areas (the taiga or boreal forest region) because the microwave emission from the trees overwhelms scattering from the underlying snowpack. With the inclusion of a forest factor in the new algorithm, considerably more SWE was estimated in these regions. The old algorithm (1) slightly underestimated SWE (by about 30 mm) in the tundra in October. In November, (1) overestimated SWE in the tundra by approximately 30 mm—the snow crystals are typically larger here in late fall and winter than in early autumn. As the snow cover extended southward into the taiga, the old algorithm underestimated SWE in excess of 60 mm in portions of the Yukon Territory and Mackenzie River Basin. In other areas of the boreal forests, the underestimation is less than 30 mm. By January 1991, positive differences are evident throughout the taiga (greater than 90 mm in places) and maritime classes as well as in the southern Rocky Mountains.

The maps for January, February, and March are very similar to each other. In the extreme northern reaches of the taiga, the new algorithm showed as much as 180 mm more SWE than did the old algorithm. In general, the increase was between about 30 and 120 mm in most forested areas. In terms of snow depth, on average, this means that in the

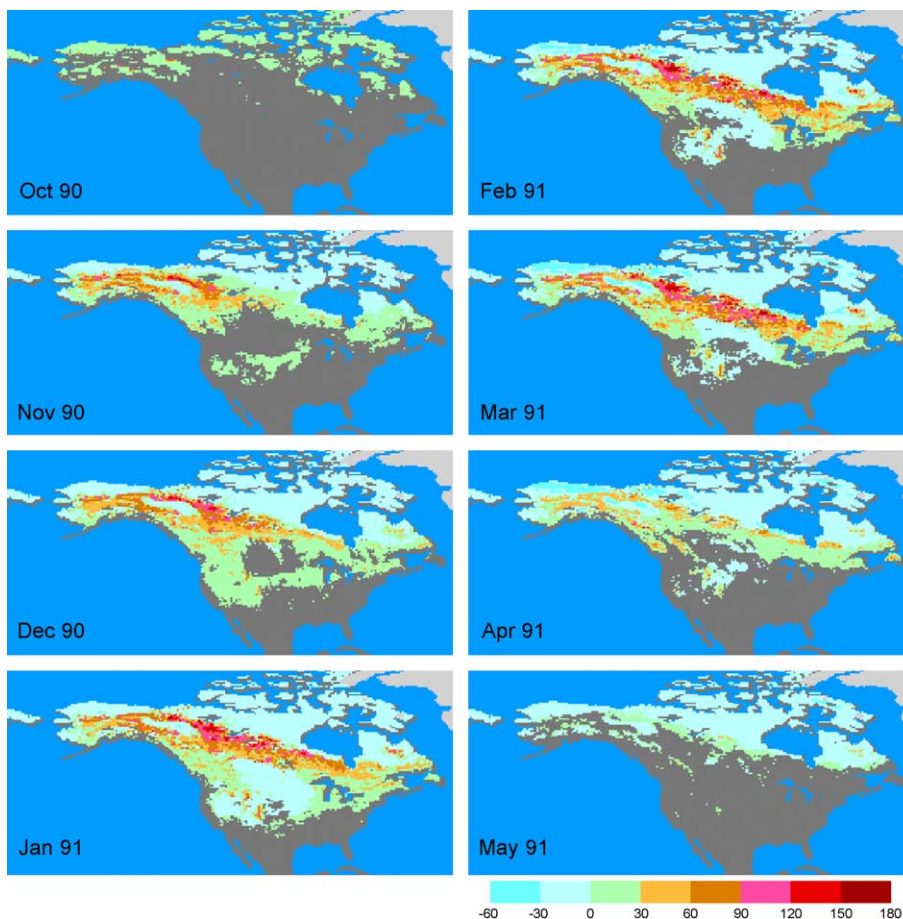


Fig. 6. Difference maps between the new and old SSM/I SWE algorithms for October 1990 through May 1991.

maritime, alpine and taiga Sturm snow classes, there is approximately 27 cm more snow on the ground using the new algorithm than using the original algorithm (using a density value of 300 kg/m). In April, the differences within the forested regions were still positive but smaller than in mid winter. For this month, maximum values in the taiga were near 90 mm. By May, the tundra was still completely snow covered, but only the northern portions of the taiga contained snow. The largest underestimation in the taiga was approximately 30 mm, whereas in the tundra, the largest overestimation by (1) was also 30 mm.

5.3. SWE retrieval uncertainty

Here we quantify the uncertainty associated with the new algorithm (9) using (11). Denoting the retrieval of SWE from the new algorithm as “observations,” as when used in data assimilation systems that assimilate SWE retrievals, we estimate the errors associated with retrieved SWE using (11). Fig. 7 illustrates the uncertainty in SWE estimates during the course of the snow accumulation and ablation period of 1990–1991. The errors are typically greatest where the snow is the deepest, the forests are most dense, and the crystals are growing the fastest. Of course, errors are

encountered even in open areas where the snow is relatively shallow; these smaller errors can be significant over continental-scale areas. The emphasis in this study though is to minimize the large errors attributable to forests and grain size.

In October 1990, errors in the tundra zone, were generally less than 12 mm. By November, the greatest errors were found in Alaska, and in the Yukon Territory and the Northwest Territories of Canada—in the tundra and along parts of the northern fringes of the taiga or boreal forest. The maximum errors here approached 24 mm. In these areas, and at this time, the snow rapidly accumulates, and snow crystals within the snowpack begin to grow as temperature gradients between the air/snow interface and the surface/snow interface are considerable (may be in excess of 25°C). By December, in the northwestern quadrant of North America, the maximum errors were actually somewhat smaller than in November. However, rather large errors (greater than about 12 mm) were found throughout the taiga. The errors in January were similar to December except that errors in the northern prairies had increased to between 6 and 9 mm. In February and March, the error maps were in close accord with the January map; however, the errors in the northern prairies were slightly less

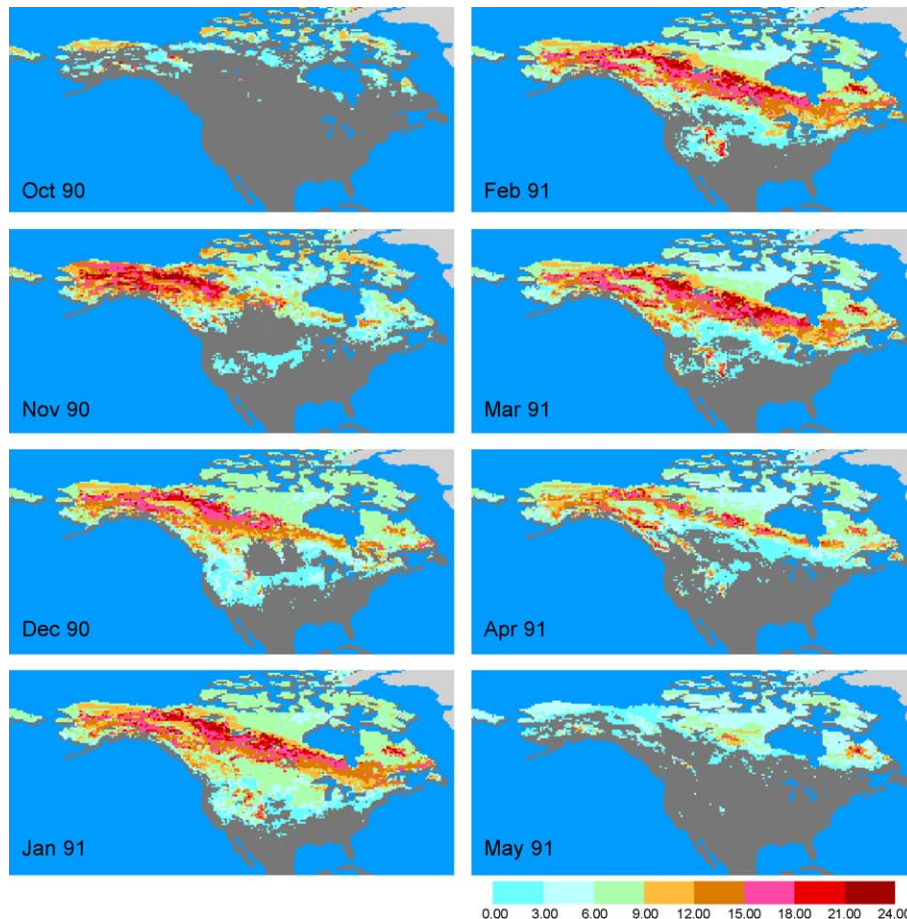


Fig. 7. Uncertainty associated with the new SSM/I SWE algorithm (9) for October 1990 through May 1991.

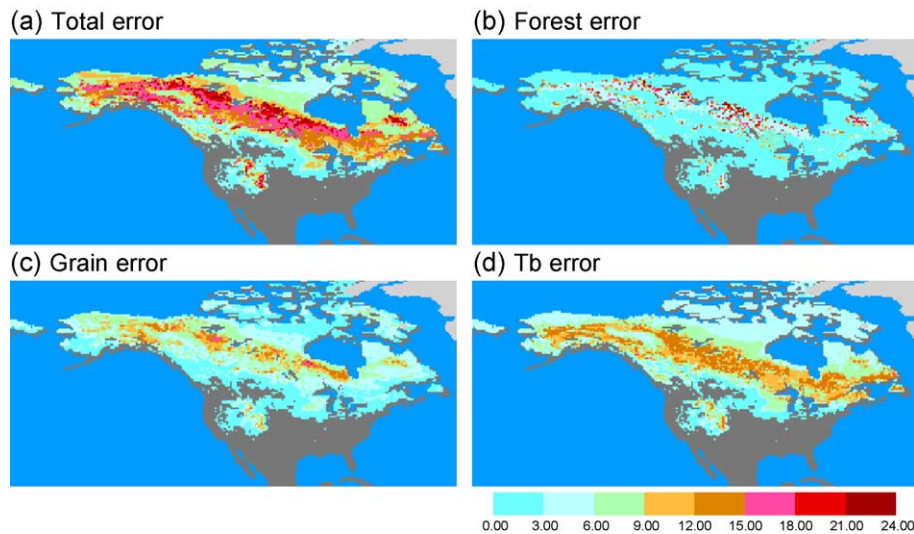


Fig. 8. (a) Total error, (b) forest error, (c) grain error, and (d) Tb error associated with the new SSM/I SWE algorithm for February 1991.

(less than 3 mm). By April, in the taiga, the geographic area of the largest errors (greater than 18 mm) was quite a bit smaller than was the case during the winter months, and by May, maximum errors exceeded 9 mm only in the northern reaches of the taiga in north central Canada as well as in northern Quebec and in northern Newfoundland.

Fig. 8 shows the breakdown of contributions from different terms in (11) for the SWE estimate by the new algorithm for February 1991. Fig. 8a shows the total error. Fig. 8b shows the contribution to this error from the impact of forest cover. These errors were generally small throughout North America (<3 mm), except within the taiga, where errors were as high as 24 mm. Fig. 8c shows that contribution to the total error due to uncertainty in crystal size, especially in portions of the tundra, the taiga, and the southern Rocky Mountains—grain size errors range from 9 to 18 mm. Fig. 8d shows the contribution to the total error resulting from brightness temperature instrument accuracy. They were greatest where the snow was the deepest in forested areas. Maximum errors in taiga, maritime, and alpine classes exceeded 12 mm. Note that since errors due to forest cover and snow crystal evolution have been corrected in the new algorithm (9), the major error left is the contribution of measurement error by the instruments.

6. Validation

We first compared the SSM/I retrievals from the old and new algorithm with in situ SWE data for the snow season 1990–1991. We then validated (9) using SSM/I data and ground SWE data from MSC for the years 1988–1995. For the purpose of validating our results, we obtained biweekly meteorological SWE data from both meteorological stations and snow courses, which were collected and analyzed by MSC (Brown et al., 2003). The snow depth data from meteorological observing stations have been converted to

SWE using snow density values interpolated from the smaller number of snow survey courses—spatially and temporally sensitive constants of density were used (Brown, 1996). The Brown et al. (2003) SWE dataset is considered the most reliable large-scale snow dataset available for Canada (Brown & Goodison, 1996). It was found by Brown et al. (2003) that SWE values from the snow depth network agreed very closely with SSM/I-derived SWE over the Canadian prairies. Mote et al. (2003) reached a similar conclusion; however, the agreement was not as favorable in forested environments.

Fig. 9 shows the location of these meteorological stations in the MSC SWE dataset. Although there are hundreds of reliable meteorological stations in southern Canada, comparatively few stations (less than 100) exist north of 55°N. However, there are sufficient stations to quantitatively evaluate the SSM/I passive microwave estimates of SWE in the above listed *Sturm* classes, except the ephemeral class that does not exist in Canada. Because our interest and focus is on the impact of both vegetation cover and crystal size differences, we have slightly modified the map derived by Sturm in the boreal forest

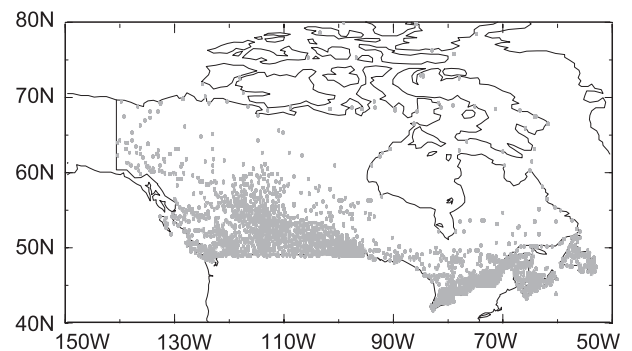


Fig. 9. Meteorological stations used in the in situ SWE dataset produced by the Meteorological Services of Canada.

region. Despite the nomenclature in the *Sturm* classes (taiga, tundra, alpine, prairie), they are not necessarily defined by vegetation characteristics (Sturm et al., 1995). For example, seasonal snowpacks with forest cover less than 80% also comprise the taiga class in the Sturm classification. After the modification, the taiga class now includes only those areas that are over 80% forested, and the tundra class includes only those less than 50% forested. A pixel classified as taiga but with less than 80% forest cover, or a pixel classified as tundra but with over 50% forest cover, is now binned into a separate tundra/taiga class.

For each station, the nearest SSM/I pixel was identified. If there exists multiple stations in one SSM/I pixel, the station data were averaged. Then, the in situ SWE data were compared to the satellite SWE retrieval using the old algorithm (1). We used this comparison during the 1990–1991 snow season to fine-tune the new SWE algorithm (9) and the uncertainty associated with it. Fig. 10 shows the comparison among SSM/I retrieval from (1) and (9) and how they compared with station SWE in each Sturm class during the 1990–1991 snow season. The number of stations with data in 1990–1991 season in each Sturm class is: 67

(tundra), 116 (taiga), 319 (prairie), 476 (alpine), and 838 (maritime). The separate class tundra/taiga (for fractional forest cover less than 80% but greater than 50%) includes 131 meteorological stations.

In general, the new algorithm (9) performs well and captures the timing of snow accumulation and ablation phases in most Sturm classes, which is very important for water resource management and flood forecasting. The SWE estimates using the old algorithm (1) compare favorably to the station data and the new algorithm (9) in the tundra and prairie classes, but systematically underestimate SWE in the taiga, alpine, and maritime classes. In the tundra, (1) actually matches the station data a little more closely than does (9) during the 2nd half of the snow season. This may be explained by the paucity of data (snow courses) here compared to the other classes, resulting in interpolated densities that are not characteristic of late winter tundra snowpacks. For example, it can be seen that the station data shows in excess of 50 mm SWE at the end of May. While a number of stations likely reported snow on the ground, it would be unusual for the entire tundra area to be snow-covered this late in the spring to a depth that would result in 50 mm of SWE.

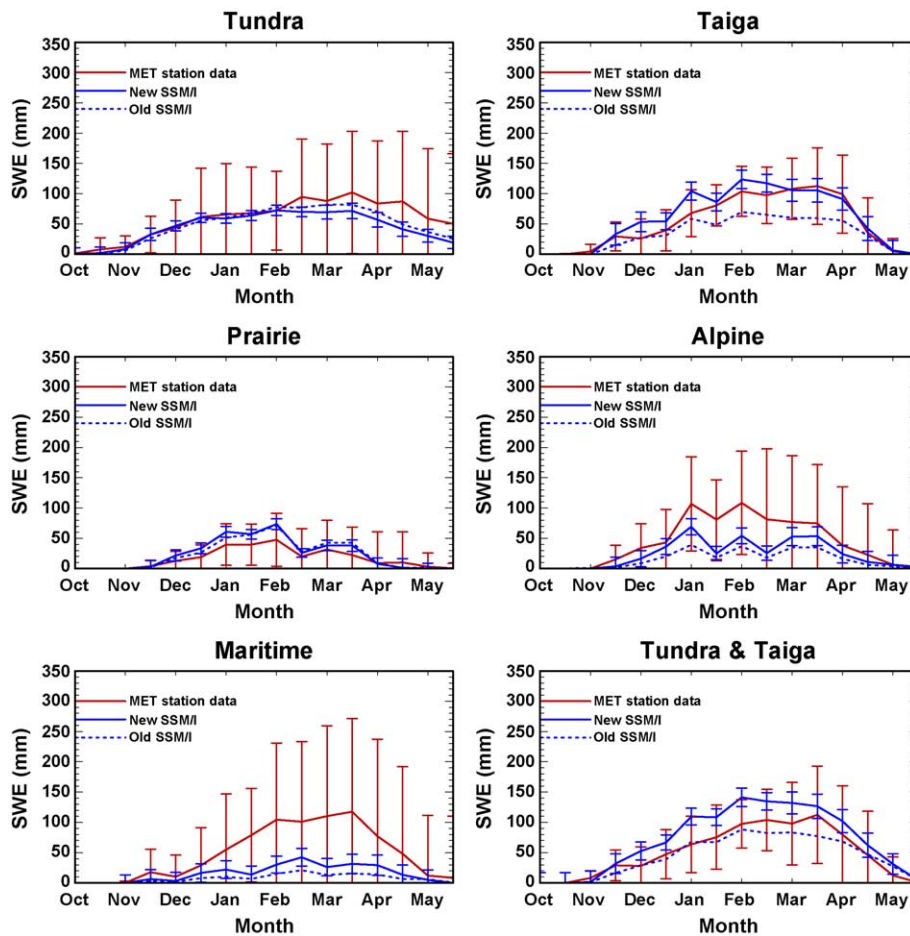


Fig. 10. Comparison of biweekly observed in situ SWE (red line) and SSM/I retrievals using the new (solid blue line) and old algorithms (dotted blue line) for the 1990–1991 snow season. Red color bars denote standard deviations of the in situ data. Blue error bars represent SSM/I SWE uncertainty.

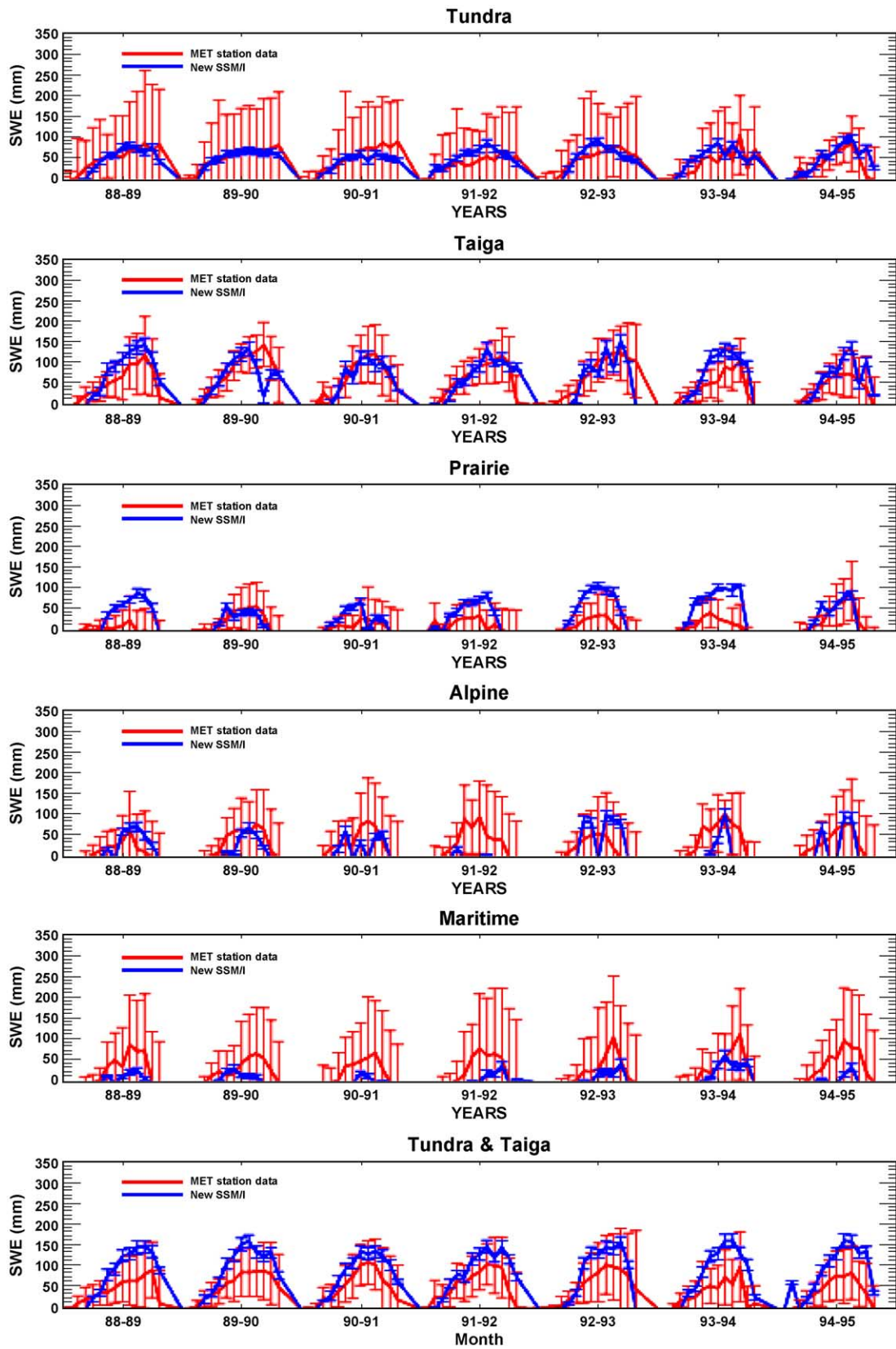


Fig. 11. Comparison of biweekly observed in situ SWE (red) and SSM/I retrieval using the new algorithm (blue) for the 1988–1995 snow seasons. Red color bars denote standard deviation of in situ data. Blue error bars represent SSM/I SWE uncertainty.

Note the considerable improvement in (9) compared to (1) in the taiga class, and to a lesser extent, the performance of (9) is better in the alpine and maritime classes. Nonetheless, the new algorithm (9) still has difficulty in adequately compensating for SWE underestimation in very dense forests of the maritime class of eastern Canada as well as alpine areas adjacent to the Great Lakes. Part of the reason for this may be attributed to the fact that many of the SSM/I pixels in the maritime and alpine class are in close proximity to water bodies—pixel contamination by open water adversely affects the evaluation. Moreover, this class is generally warmer than the other classes (except for the ephemeral class), and the warmer and wetter snow, results in smaller brightness temperature differences between the 19 and 37 GHz frequencies, and therefore lesser PM-derived snow amounts. Further study on this issue is needed.

Fig. 11 shows the comparison of SSM/I SWE and ground SWE data using (9) for different Sturm classes during the 1988–1995 period. The root-mean-square (RMS) errors of the observed SWE and our uncertainty estimates for SSM/I SWE are also shown. While year-to-year differences can be observed for each of the classes, nevertheless the passive microwave derived SWE is, in general, concordant with SWE obtained from station data. Note that, for almost every year, the SWE retrieval from the new algorithm (9) matches very well with the station data in the Tundra and Taiga classes.

In only a few instances are the SSM/I SWE values clearly outside of the RMS limits, in the taiga class during 1994–1995 and in the prairie class during 1993–1994, for example. Note the difference in the prairie class between 1993, 1994, and 1995. The greater disagreement in 1992–1993 and 1993–1994 may be attributable to larger temperature gradients during those winters, which resulted in bigger crystals (and or more extensive depth hoar). If this were the case, then the SWE derived from the SSM/I observations would have overestimated the actual SWE.

7. Discussion

It should be noted that the in situ SWE dataset has been quality-controlled, and that the agreement between the station data and satellite-derived estimates give credence to the quality of our new algorithm as a first step towards a more comprehensive estimation of SWE. However, it needs to be emphasized that care is required when comparing point data (from meteorological stations) with areal measurements (from satellites) since point data, particularly in data sparse areas of central and northern Canada, may not be representative of the area covered by large PM footprints. The large standard deviations of point data in Sturm classes are prominent in Figs. 10 and 11, especially for the tundra, alpine, and maritime classes. Although using point data may not be ideal, nonetheless, for sufficiently large number of point data in a pixel, a meaningful validation could be achieved. A

snow dataset for all of North America, using density values from a simple snowpack model has been developed by the Meteorological Service of Canada; it may be more advantageous for future evaluation of SWE over the entire continent (Armstrong & Brown, personal communication).

The impact of vegetation cover on the SWE measurement by passive microwave sensors depends on the type and density of vegetations, not only the percentage of forest cover at each pixel. In this study, we take a simple approach by parameterizing the error based on fractional forest cover at each pixel. When better forest density data emerges, the impact of vegetation on passive microwave emission can be better modeled or parameterized. Furthermore, the forest factor derived here does not vary with latitude or with species. A more detailed classification of forests may be necessary to account for the impact of vegetation cover on SWE retrieval by passive microwave sensors. Derksen et al. (2003) empirically derived PM SWE separately for four kinds of land cover within each pixel, and found that the predominantly forested areas were most difficult to get accurate estimates of PM SWE. As more complete data on forest density becomes available, separate forest factors could be prescribed for taiga, alpine, and maritime subclasses to better account for SWE in densely forested areas.

In the most densely forested areas of the taiga class of eastern Canada as well as the maritime class of eastern Canada and the northeastern U.S. and in the alpine class in south central Canada, SWE is still underestimated using the new algorithm. To correct for PM underestimation of SWE in densely forested areas is a very challenging problem.

Because very little work has been done thus far in terms of collection and analyzing crystals in the different Sturm classes of North America, a rigorous validation of the PM errors due to crystal evolution is not yet possible. While crystals have been collected in each of the Sturm classes, only a few samples have been collected for quantitative examination by electron microscopy. Moreover, the samples that have been collected have only been gathered in late winter and early spring, not throughout the snow season. Nevertheless, the results presented here give us confidence regarding the validity of PM-derived snow estimates, especially during the accumulation and ablation phases of snow season.

Analyzing data collected during the Cold Land Processes Field Experiment (CLPX) in the winter of 2002 and 2003 in the Colorado Rocky Mountains will help quantify the uncertainty in the PM-derived snow estimates (Cline et al., 2002). One reason the Colorado Rocky Mountain area was selected is that it encompasses several Sturm snow classes (taiga, alpine and prairie). In addition, aircraft experiments planned during the winter of 2006 in northern Alaska and Canada should be useful for better characterizing snow crystals in the tundra region. The methodology proposed in this study can be applied to the AMSR-E SWE data to obtain error estimates, and CLPX observations should significantly enhance these estimates. The potential

benefits of using AMSR-E data have been discussed in detail in Kelly et al. (2003).

We only presented the results from SSM/I data for North America here, since there are more in situ SWE data on this continent than anywhere in the world, and the relative abundance of field campaigns and in situ SWE measurements provide insight to snow crystal structure. A future study will extend our analysis to the rest of the world (Eurasia and South America). Methodically, it is straightforward to apply it globally, but careful validation and tuning of empirical error estimates based on the “ground truth” are needed. To produce a long time series of continuous SWE data and coherent error estimation, by combining SMMR and SSM/I data, some consideration is needed to merge them seamlessly (see for example Derksen & Walker, 2003). Instrument differences between the sensors and small differences in the overpass time and incidence angle between SMMR and SSM/I (Table 1) could influence SWE retrieval in a systematic manner (Derksen et al., 2000). Armstrong and Brodzik (2001) have shown that a 5K difference in the $(T_{19}-T_{37})$ term exists between SMMR and SSM/I SWE retrieval when using (1). Nevertheless, the methodology used here could be easily applied to SSMR to study its SWE retrieval and associated errors. This subject is the focus of an on-going study.

8. Conclusions

We propose a new passive microwave SWE retrieval algorithm based on the original algorithm by Chang et al. (1987) that accounts for the effect of vegetation cover and snow morphology in the North America. The contributions to the microwave response of snow by various factors are examined and evaluated. Dense vegetation is shown to be the major source of systematic error in the old algorithm; the assumption of constant snow grain size also contributes significant errors. Simplified empirical formulas are used to quantify the impact of vegetation cover and grain size growth during the snow season.

The results have been evaluated in tundra, taiga, prairie, alpine, and maritime Sturm classes in Canada using in situ SWE data from the Meteorological Service of Canada. The new algorithm reduces known biases in the old algorithm in most areas (particularly in taiga) and is shown to capture the accumulation and ablation phases of snow season well. The snow season during 1990–1991 is used as a case study. Seven snow seasons from 1988–1995 are evaluated. There is still some difficulty with the alpine and maritime Sturm classes, and partially forested areas. Recent field campaigns such as CLPX will help improve the parameterization of the passive microwave SWE retrievals. The improved spatial resolution and expanded range of channels at lower frequencies of the AMSR-E instrument will help curb the problems associated with mixed pixels and enhance the detection of shallow snowpacks.

We applied a methodology based on error estimation theory to quantify SSM/I SWE retrieval errors when using the new algorithm (9). The assessment of impact by forest cover and snow grain size are empirical based on our understanding of the nature of passive microwave emission from the ground. These empirical formulas need to be rigorously validated and updated when more extensive and accurate in situ observations become available; nonetheless, the methodology proposed here provides a means to evaluate the uncertainty in passive microwave SWE retrievals. Future study will investigate global application of our methodology and extend back to SSMR data (1979) to produce a long time series (over 25 years) of PM SWE data and coherent error estimates.

Acknowledgements

The authors thank Matthew Sturm for providing digitized data for the six snow classes and the image of Fig. 1. We also thank Ross Brown for providing the in situ SWE dataset of the Meteorological Services of Canada. Helpful comments by the three anonymous reviewers are gratefully acknowledged (especially Reviewer 2 for detailed and insightful comments). This work was supported by the NASA Earth Observing System Interdisciplinary Science (NASA EOS/IDS) Program NRA99-OES-04.

References

- Armstrong, R. L., & Brodzik, M. J. (1995). An earth-gridded SSM/I data set for cryospheric studies and global change monitoring. *Advances in Space Research*, 10, 155–163.
- Armstrong, R. L., & Brodzik, M. J. (2001). Recent Northern Hemisphere snow extent: A comparison of data derived from visible and microwave satellite sensors. *Geophysical Research Letters*, 28, 2676–2679.
- Brown, R. D. (1996). Evaluation of methods for climatological reconstruction of snow depth and snow cover duration at Canadian meteorological stations. *Proc. Eastern Snow Conf., 53rd Annual Meeting* (pp. 55–65). Williamsburg, VA.
- Brown, R., Brasnett, B., & Robinson, D. (2003). Gridded North American monthly snow depth and snow water equivalent for GCM evaluation. *Atmosphere-Ocean*, 41, 1–14.
- Brown, R. D., & Goodison, B. E. (1996). Interannual variability in reconstructed Canadian snow cover, 1915–1992. *Journal of Climate*, 9, 1299–1318.
- Chang, A. T. C., Foster, J. L., & Hall, D. K. (1986). Microwave snow signatures (1.5 mm to 3 cm) over Alaska. *Cold Regions Science and Technology*, 13, 153–160.
- Chang, A. T. C., Foster, J. L., & Hall, D. K. (1987). Nimbus-7 derived global snow cover parameters. *Annals of Glaciology*, 9, 39–44.
- Chang, A. T. C., Foster, J. L., & Hall, D. K. (1996). Effects of forest on the snow parameters derived from microwave measurements during the BOREAS winter field experiment. *Hydrological Processes*, 10, 1565–1574.
- Chang, A. T. C., Foster, J. L., Hall, D. K., Rango, A., & Hartline, B. (1982). Snow water equivalent determination by microwave radiometry. *Cold Regions Science and Technology*, 5, 259–267.

- Chang, A. T. C., Foster, J. L., Owe, M., Hall, D. K., & Rango, A. (1985). Passive and active microwave studies of snowpack properties, results of March, 1981 Aircraft Mission. *Nordic Hydrology*.
- Chang, A. T. C., Gloersen, P., Schmugge, T., Wilheit, T., & Zwally, J. (1976). Microwave emission from snow and glacier ice. *Journal of Glaciology*, 16, 23–39.
- Chang, A. T. C., & Rango, A. (2000). Algorithm Theoretical Basis Document (ATBD) for the AMSR-E Snow Water Equivalent Algorithm. NASA/GSFC, Nov. 2000.
- Cline, D., Armstrong, R., Davis, R., Elder, K., & Liston, G. (2002). Cold land processes field experiment. In M. Parsons, & M. J. Brodzik (Eds.), *Digital media*. Boulder, CO: National Snow and Ice Data Center.
- Colbeck, S. C. (1982). An overview of seasonal snow metamorphism. *Reviews of Geophysics and Space Physics*, 20, 45–61.
- Derksen, C., & Walker, A. (2003). Identification of systematic bias in the cross-platform (SMMR and SSM/I) EASE-Grid brightness temperature time series. *IEEE Transactions on Geoscience and Remote Sensing*, 41(4), 910–915.
- Derksen, C., LeDrew, E., Walker, A., & Goodison, B. (2000). The influence of sensor overpass time on passive microwave retrieval of snow cover parameters. *Remote Sensing of Environment*, 71(3), 297–308.
- Derksen, C., Walker, A., & Goodison, B. (2003). A comparison of 18 winter seasons of in situ and passive microwave-derived snow water equivalent estimates in Western Canada. *Remote Sensing of Environment*, 88(3), 271–282.
- Foster, J. L., Chang, A. T. C., Hall, D. K., & Rango, A. (1991). Derivation of snow water equivalent in boreal forests using microwave radiometry. *Arctic*, 14, 147–152.
- Foster, J. L., Hall, D. K., Chang, A. T. C., Rango, A., Wergin, W., & Erbe, E. (1999). Effects of snow crystal shape on the scattering of passive microwave radiation. *IEEE Transactions on Geoscience and Remote Sensing*, 37(2), 1165–1168.
- Foster, J. L., et al. (1996). Snow cover and snow mass intercomparisons of general circulation models and remotely sensed data sets. *Journal of Climate*, 9, 409–426.
- Franklin, J. (1986). Thematic Mapper analysis of coniferous forest structure and composition. *International Journal of Remote Sensing*, 7, 1287–1301.
- Goita, K., Walker, A., & Goodison, B. (2003). A comparison of 18 winter seasons of in situ and passive microwave derived snow water equivalent estimates in Western Canada. *Remote Sensing of Environment*, 88(3), 271–282.
- Gong, G., Entekhabi, D., Cohen, J., & Robinson, D. (2004). Sensitivity of Atmospheric Response to Modeled Snow Anomaly Characteristics. *Journal of Geophysical Research*, 109, D06107. doi:10.1029/2003JD004160.
- Hall, D. K., Chang, A. T. C., & Foster, J. L. (1986). Detection of the depth hoar layer in the snowpack of the arctic coastal plain of Alaska using satellite data. *Journal of Glaciology*, 32, 87–94.
- Hall, D. K., Foster, J. L., & Chang, A. T. C. (1982). Measurement and modeling of microwave emission from forested snowfields in Michigan. *Nordic Hydrology*, 13, 129–138.
- Hall, D. K., Foster, J. L., Salomonson, V. V., Klein, A. G., & Chien, J. Y. L. (2001). Development of a technique to assess snow cover mapping errors from space. *IEEE Transactions on Geoscience and Remote Sensing*, 39, 432–438.
- Hall, D. K., Kelly, R. E. J., Riggs, G. A., Chang, A. T. C., & Foster, J. L. (2002). Assessment of the relative accuracy of hemispheric-scale snow-cover maps. *Annals of Glaciology*, 34, 24–30.
- Hall, D. K., Sturm, M., Benson, C. S., Chang, A. T. C., Foster, J. L., Garbeil, H., et al. (1991). Passive microwave remote and in-situ measurements of Arctic and Subarctic snow covers in Alaska (March 1988). *Remote Sensing of Environment*, 88, 161–172.
- Heuvelink, G. B. M. (1998). *Error propagation in environmental modeling with GIS* (p. 144). Taylor & Francis.
- Kelly, R. E. J., & Chang, A. T. C. (2003). Development of a passive microwave global snow depth retrieval algorithm for SSM/I and AMSR-E data. *Radio Science*, 38(4), 8076. doi:10.1029/2002RS002648.
- Kelly, R., Chang, A., Tsang, L., & Foster, J. (2003). A prototype AMSR-E global snow area and snow depth algorithm. *IEEE Transactions on Geoscience and Remote Sensing*, 41(2), 230–242.
- Loveland, T. R., Reed, B. C., Brown, J. F., Ohler, D. O., Zhu, J., Yang, L., et al. (2000). Development of a global land cover characteristics dataset. *International Journal of Remote Sensing*, 21(6/7), 1303–1330.
- Matzler, C. (1987). Passive microwave signatures of landscapes in winter. *Meteorology and Atmospheric Physics*, 54, 241–260.
- Matzler, C., & Standley, A. (2000). Relief effects for passive microwave remote sensing. *International Journal of Remote Sensing*, 21, 2403–2412.
- Mote, T. L., Grundstein, A. J., Leathers, D. J., & Robinson, D. A. (2003). A comparison of modeled, remotely sensed and measured snow water equivalent in the northern Great Plains. *Water Resources Research*. doi:10.1029/2002WR001782.
- NOAA/NESDIS. (1990 and 1991). Weekly Snow Cover Maps of the Northern Hemisphere, October–May.
- Pulliaainen, J., & Hallikainen, M. (2001). Retrieval of regional snow water equivalent from space-borne passive microwave observations. *Remote Sensing of Environment*, 75, 76–85.
- Rango, A. (1983). A survey of progress in remotes sensing of snow and ice. *Proceedings of the international symposium on remote sensing and remote data transmissions*. Hamburg, Germany: International Association of Hydrologic Science.
- Rango, A., Chang, A., & Foster, J. (1979). The utilization of space-borne radiometers for monitoring snowpack properties. *Nordic Hydrology*, 10, 25–40.
- Robinson, D. A., & Kukla, G. (1985). Maximum surface albedo of seasonally snow covered lands in the Northern Hemisphere. *Journal of Climate and Applied Meteorology*, 24, 402–411.
- Robinson, D. A., Dewey, K. F., & Heim, R. R. (1993). Global snow cover monitoring: An update. *Bulletin of the American Meteorological Society*, 74, 1689–1696.
- Schmugge, T. (1980). Techniques and applications of microwave radiometry. In B. S. Siegal, & A. R. Gillespie (Eds.), *Remote sensing in geology* (pp. 337–352). New York: Wiley (Chap. 11).
- Scialdone, J., & Robuck, A. (1987). Comparison of Northern Hemisphere snow cover data sets. *Journal of Climate and Applied Meteorology*, 26, 53–68.
- Sturm, M., Holmgren, J., & Liston, G. E. (1995). A seasonal snow cover classification system for local to regional applications. *Journal of Climate*, 8, 1261–1283.
- Sun, C., Walker, J. P., & Houser, P. R. (2004). A methodology for snow data assimilation in a land surface model. *Journal of Geophysical Research*, 109, D08108. doi:10.1029/2003JD003765.
- Tsang, L., Chen, C., Chang, A. T. C., Guo, J., & Ding, K. (2000). Dense media radiative transfer theory based on quasicrystalline approximation with applications to passive microwave remote sensing of snow. *Radio Science*, 35, 731–749.
- Ulaby, F. T., & Stiles, W. H. (1980). The active and passive microwave response to snow parameters: 2. Water equivalent of dry snow. *Journal of Geophysical Research*, 85(C2), 1045–1049.
- Walker, A., & Goodison, B. (1993). Discrimination of a wet snow cover using passive microwave satellite data. *Annals of Glaciology*, 17, 307–311.
- Wiesman, A., & Mätzler, C. (1999). Microwave emission model of layered snowpacks. *Remote Sensing of Environment*, 70, 307–316.